

Chemical Science

Accepted Manuscript

This article can be cited before page numbers have been issued, to do this please use: D. Jansen, J. Gramueller, F. Niemeyer, T. Schaller, M. C. Letzel, S. Grimme, H. Zhu, R. M. Gschwind and J. Niemeyer, *Chem. Sci.*, 2020, DOI: 10.1039/D0SC01026J.



This is an Accepted Manuscript, which has been through the Royal Society of Chemistry peer review process and has been accepted for publication.

Accepted Manuscripts are published online shortly after acceptance, before technical editing, formatting and proof reading. Using this free service, authors can make their results available to the community, in citable form, before we publish the edited article. We will replace this Accepted Manuscript with the edited and formatted Advance Article as soon as it is available.

You can find more information about Accepted Manuscripts in the [Information for Authors](#).

Please note that technical editing may introduce minor changes to the text and/or graphics, which may alter content. The journal's standard [Terms & Conditions](#) and the [Ethical guidelines](#) still apply. In no event shall the Royal Society of Chemistry be held responsible for any errors or omissions in this Accepted Manuscript or any consequences arising from the use of any information it contains.

ARTICLE

What is the Role of Acid-Acid Interactions in Asymmetric Phosphoric Acid Organocatalysis? A Detailed Mechanistic Study using Interlocked and Non-Interlocked Catalysts⁵

Dennis Jansen,^a Johannes Gramüller,^b Felix Niemeyer,^a Torsten Schaller,^a Matthias C. Letzel,^c Stefan Grimme,^d Hui Zhu,^{*d} Ruth M. Gschwind,^{*b} and Jochen Niemeyer^{*a}Received 00th January 20xx,
Accepted 00th January 20xx

DOI: 10.1039/x0xx00000x

Organocatalysis has revolutionized asymmetric synthesis. However, the supramolecular interactions of organocatalysts in solution are often neglected, although the formation of catalyst aggregates can have a strong impact on the catalytic reaction. For phosphoric acid based organocatalysts, we have now established that catalyst-catalyst interactions can be suppressed by using macrocyclic catalysts, which react predominantly in a monomeric fashion, while they can be favored by integration into a bifunctional catenane, which react mainly as phosphoric acid dimers. For acyclic phosphoric acids, we found a strongly concentration dependent behavior, involving both monomeric and dimeric catalytic pathways. Based on a detailed experimental analysis, DFT-calculations and a direct NMR-based observation of the catalyst aggregates, we could demonstrate that intermolecular acid-acid interactions have a drastic influence on the reaction rate and stereoselectivity of the asymmetric transfer-hydrogenation catalyzed by chiral phosphoric acids.

Introduction

Many organocatalysts, such as amines, diols, amino-acid derivatives, (thio)ureas or phosphoric acids are highly functionalized organic molecules, oftentimes featuring hydrogen-bond donor and acceptor moieties or even Brønsted-acidic and Brønsted-basic functional groups within the same molecule.^[1] Also, many organocatalytic reactions rely on the use of high catalyst loadings and are performed in aprotic organic solvents.^[2,3,4] This makes the formation of aggregates highly likely, be it catalyst•catalyst aggregates or higher-order catalyst•catalyst•substrate aggregates. The comprehension and control of such aggregation processes would not only enable a better understanding of organocatalytic processes, but also open up new possibilities in catalysis, when such catalyst aggregates can be designed and applied in a controlled fashion.

In previous works, aggregation of organocatalysts was observed in a few cases: In urea-catalysis, Jacobsen has shown that catalyst-catalyst interactions can both be detrimental or beneficial.^[5] The identification of a cooperative substrate activation in a catalyst•catalyst•substrate complex led to the

development of tethered^[6] and macrocyclic^[7] bis-urea catalysts. Supramolecular catalyst aggregation has also been observed for chincona-alkaloid based organocatalysts, in this case leading to catalyst deactivation and decreased enantioselectivities.^[8] In case of BINOL-based phosphoric acids,^[9] Gong showed that acid-acid interactions lead to a different solubility of the racemic and the homochiral catalyst species, resulting in strong nonlinear effects.^[10] Phosphoric acid aggregation has also been proven by spectroscopic means: Dimers and trimers of dimethylphosphoric acid were identified by NMR^[11] and Hunger could show the presence of multimers for complexes of diphenyl phosphoric acid and a quinoline.^[12] For chiral phosphoric acids (CPA) with a BINOL-backbone, extended aromatic surfaces allow additional weak non-covalent interactions, which further stabilize hydrogen-bonded catalyst•substrate complexes,^{[13],[14]} and can also enable the formation of higher aggregates, such as dimers of CPA•imine complexes.^[15]

We recently found that integration of two BINOL-phosphoric acids in a catenane structure^[16] leads to drastic changes both in reaction rates and stereoselectivities for the transfer hydrogenation of quinolines. DFT-calculations suggested that a hydrogen-bond mediated acid-acid interaction^{[17],[18]} leads to a more stereoselective dimeric catalyst pathway (featuring two acids and both substrates), as opposed to a less stereoselective monomeric pathway (involving one acid and both substrates).

We thus concluded that the mechanical interlocking of two phosphoric acids is an effective mean to channel the reaction

^a Faculty of Chemistry (Organic Chemistry) and Center for Nanointegration Duisburg-Essen (CENIDE), University of Duisburg-Essen, Universitätsstrasse 7, 45141 Essen, Germany

^b Organic Chemistry, University of Regensburg, 93040 Regensburg, Germany

^c Institute of Organic Chemistry, University of Münster, Corrensstrasse 40, 48149 Münster, Germany

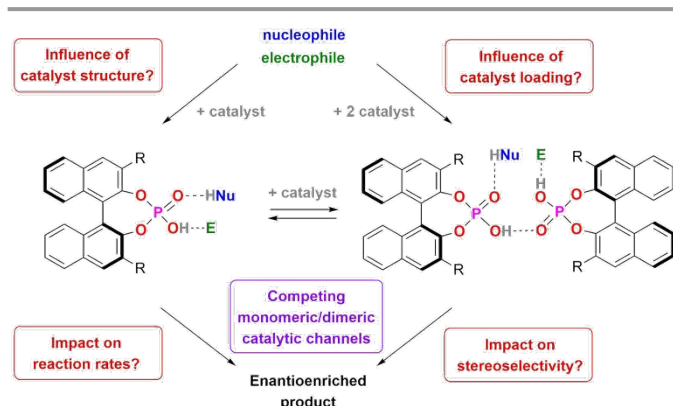
^d Mulliken Center for Theoretical Chemistry, Rheinische Friedrich-Wilhelms Universität Bonn, Beringstrasse 4, 53115 Bonn, Germany.

* Electronic Supplementary Information (ESI) available: See

DOI: 10.1039/x0xx00000x

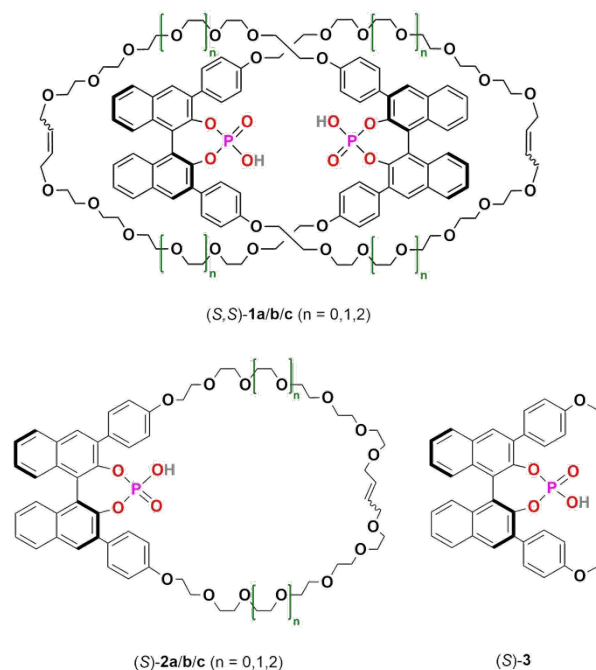


through the dimeric pathway, but of course other factors that lead to increased acid-acid interactions (such as higher catalyst loadings) might have a similar effect (Scheme 1). This could impact the outcome of a large range of asymmetric transformations that are mediated by chiral Brønsted-acids.



Scheme 1: Key questions for this investigation

For this reason, we have now performed a detailed mechanistic study, trying to shed light on these effects. We investigated the influence of catalyst structure and loading, using catenated, macrocyclic and acyclic phosphoric acids as catalysts (catalysts **1/2/3**, scheme 2). This enabled us to understand how the competing catalytic pathways impact the catalytic reaction in terms of reaction rates and stereoselectivities, thus demonstrating the importance of acid-acid interactions in Brønsted-acid organocatalysis.



Scheme 2: Catenated catalysts (S,S)-**1a/b/c**, macrocyclic catalysts (S)-**2a/b/c** and acyclic catalyst (S)-**3** used in this study

Results and discussion

View Article Online

DOI: 10.1039/D0SC01026J

General approach

The reactivity and stereoselectivity of the three different catalysts was investigated using the reduction of 2-phenylquinoline (**4**) with dihydropyridine **7** (Hantzsch-ester) to give tetrahydroquinoline **6** and pyridine **8** (table 1). The reaction was carried out in toluene at 25 °C, as established previously.^[17]

Time-resolved data was obtained by NMR-spectroscopy. Rate constants were determined both by nonlinear fitting^[19] and linear fitting of the conversion plots, which gave almost identical results (SI table S4-S7 and chapter 9). We also performed progress kinetic analysis (RPKA) based on different and same excess measurements.^[20] Mechanistic information was obtained by variable time normalization analysis (VTNA, see SI chapter 4.4).^{[21],[22]}

Influence of the catenane ring sizes

As a starting point, we employed catenanes **1a/b/c** with varying ring-sizes, assuming that the ring-size will influence the (mechano)intramolecular acid-acid interactions, thus effecting reaction rates and stereoselectivities. In addition to the previously reported hexaethyleneglycol-based species **1b/2b**,^[16] we generated the smaller, pentaethyleneglycol-based systems **1a/2a** and the larger, heptaethyleneglycol-based systems **1c/2c** (SI chapter 2). Interestingly, there is a clear increase in yields of both catenanes and macrocycles with increasing ring size (5%/7%/10% for **1a/b/c** and 8%/11%/15% for **2a/b/c**),^[23] suggesting that the longer linkers have a sufficient length for the intramolecular ring-closing metathesis, while the shorter linkers lead to increased formation of oligomeric byproducts.

In catalysis, the catenanes **1a/b/c** show drastically enhanced stereoselectivities in comparison to the macrocycles **2a/b/c** (as earlier reported for the **1b/2b** pair).^[17]

Table 1. Results of the transfer hydrogenation of 2-phenylquinoline with catalysts **1a/b/c** and **2a/b/c**

Catalyst ^[a]	ee [%] ^[b]	v_0 [10^{-7} M s ⁻¹]	Catalyst ^[a]	ee [%] ^[b]
(S,S)- 1a	81	3.7	(S)- 2a	-17
(S,S)- 1b	84	3.1	(S)- 2b	-12
(S,S)- 1c	82	2.0	(S)- 2c	-17

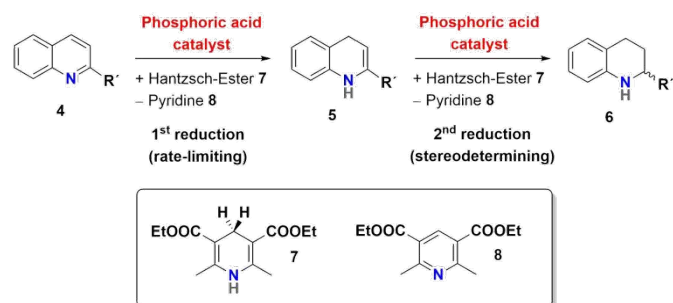
[a] 2.5 mol% catalyst, 5 mM quinoline. [b] Determined by chiral HPLC. Values given for the excess of (R)-**6**



However, there was no impact of the ring-sizes on the stereoselection: Enantiomeric excesses were in the range of 81-84% in favor of the (*R*)-product for catenanes (*S,S*)-**1a/b/c**, while the macrocycles (*S*)-**2a/b/c** consistently favored the (*S*)-product with 12-17% *ee*. However, the reaction rates of **1a/b/c** clearly depend on the ring-size, with the smaller catenanes showing higher rates ($v_0 = 3.7 \cdot 10^{-7} / 3.1 \cdot 10^{-7} / 2.0 \cdot 10^{-7} \text{ M s}^{-1}$ for **1a/b/c** at 10% catalyst loading). This suggests that the geometry of the stereodetermining transition-states is not influenced by the ring-sizes, but the reaction rates are decreased. This might be due to intramolecular hydrogen bonding of the P(O)OH-unit to the ethylene glycol units (as found in our earlier DFT work^[17]), which might be more prevalent in the larger systems.

First reduction step: Kinetic analysis

The mechanism for the phosphoric acid catalyzed transfer-hydrogenation of quinolines involves two steps (Scheme 3): First, quinoline **4** is reduced to the corresponding 1,4-dihydroquinoline **5**, followed by reduction to the chiral 1,2,3,4-tetrahydroquinoline **6**. Both steps involve activation of the substrate by protonation, followed by Hantzsch-Ester coordination, hydride-transfer and product-dissociation. Like other phosphoric acid-catalyzed reactions, the stereoselectivity of such transfer-hydrogenations strongly depends on the nature of the phosphoric acid, with bulky 3,3'-substituents allowing for high stereoselectivities.^[9] Thus, excellent selectivities were achieved even at low catalyst loadings for 2-arylquinolines^[4a] or benzoxazines^[4b] using a phosphoric acid with phenanthryl-groups in the 3,3'-positions.



Scheme 3: Two-step transfer-hydrogenation of quinolines **4** to tetrahydroquinolines **6**.

This catalytic mechanism^{[3],[24]} closely resembles the related transfer-hydrogenation of imines.^[25] Our recent DFT results support this mechanism and suggest that the rate-limiting transition state occurs in the first reduction of **4** to **5**, namely in the protonation of the 1,4-dihydroquinoline-species. In comparison, the subsequent stereoselective second reduction towards **6** has a lower barrier. Moreover, our DFT-results suggest an additional mechanistic pathway involving two phosphoric acids, which we assume in case of the catenane-catalysts **1**.^[17]

However, to the best of our knowledge, an experimental elucidation of these mechanisms has not been reported. To probe the suggested mechanism, we firstly determined the reaction orders for substrates **4** and **7** (reaction orders *m*, *n*)

and the role of product inhibition. Secondly, the order in catalyst (reaction order *p*) was determined for the catalysts **1c/2c/3**

$$v = -\frac{d[Q]}{dt} = k_{obs} \cdot [Q]^m \cdot [HE]^n = k \cdot [Cat]^p \cdot [Q]^m \cdot [HE]^n \quad (\text{eq. 1})$$

A first analysis of the time-resolved NMR-data (SI fig. S2/S3) shows that the reduction of **4** to **6** occurs selectively with no side products. The intermediate 1,4-dihydroquinoline was not observed in any of our experiments, mainly due to its high free energy (low concentration) as suggested by our recent DFT calculations.^[17] Since the reduction of **4** into **5** is rate-limiting, the reaction orders *p*, *m*, *n* describe the first reduction step from **4** to **5**.

Substrate orders and product inhibition

For the catenated catalyst **1c**, rate measurements at different concentrations of quinoline **4** and Hantzsch-ester **7** indicated a linear dependence of reaction rate on the substrate concentrations. In the resulting $\ln v_0 / \ln [\text{substrate}]$ plots (fig. 1a/b), we could determine reaction orders of 0.8 (for **4**) and 0.7 (for **7**), respectively. This is in good agreement with the VTNA-plots (fig. 1c/d, see fig. S7 for other values of *m/n*), which show excellent overlap of all curves for substrate orders of 1 for both the quinoline and the Hantzsch-ester.

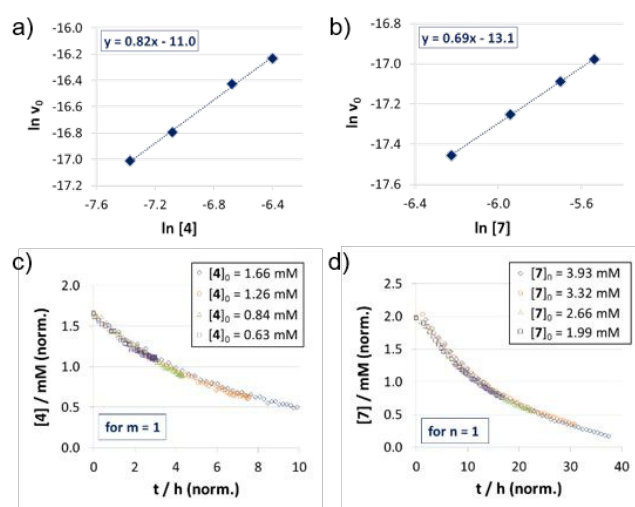


Figure 1: Substrate order determination by different excess experiments for quinoline **4** (a, c) and Hantzsch-ester **7** (b, d) in case of catenane **1c**: $\ln v_0 / \ln [\text{Substrate}]$ plots (v_0 in $\text{M}^{-1} \text{s}^{-1}$, substrate concentrations in M) (a, b) and VTNA-plots (c, d).

Accordingly, the substrate orders for the macrocyclic catalyst and acyclic catalysts **2c/3** were determined based on VTNA only. It was found that both substrates have a reaction order of close to 1 for both catalysts (SI fig. S11/S15). Thus, there is no difference with regard to the substrate orders for the different catalysts **1c/2c/3**. In addition, we performed same excess experiments in order to investigate potential catalyst deactivation or product inhibition (SI fig. S10/S14/S19). In all cases, we observed only minor differences, so that there seems to be neither catalyst deactivation nor product inhibition for all three catalysts **1c/2c/3**.



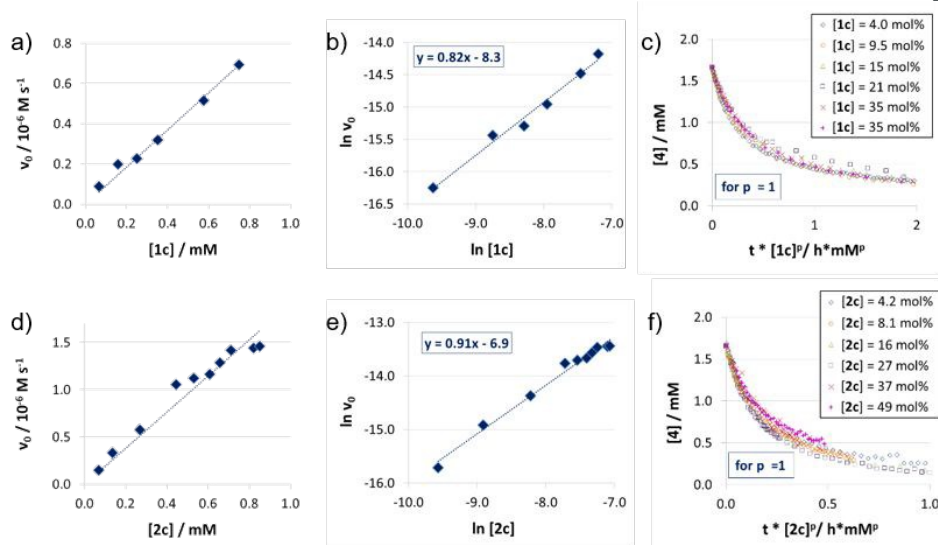


Figure 2: Catalyst order determination for catalysts **1c** (a, b, c) and **2c** (d, e, f): Initial rates (all at 1.66 mM quinoline **4** and 3.93 mM Hantzsch-ester **7**) (a, d), $\ln v_0 / \ln [\text{catalyst}]$ plots (v_0 in $\text{M}^{-1} \text{s}^{-1}$, catalyst concentrations in M) (b, d) and VTNA-plots (selected catalyst concentrations only) (c, f).

Catalyst orders and aggregation

The reaction orders of the catalysts were determined in a series of experiments with different concentrations of catalysts **1c/2c/3**. For the catenated and macrocyclic catalysts **1c/2c**, the v_0 vs. [Catalyst] plots (fig. 2a/d) clearly show a linear increase of rate upon increasing the catalyst loading in a range of 5–50 mol%. Thus, we could determine the order in catalyst based on the respective double logarithmic plots (fig. 2b/e), resulting in catalyst orders of 0.82 (for the bifunctional catenane **1c**) and 0.91 (for the monofunctional macrocycle **2c**). Once again, the first order dependence is also found by VTNA, which shows excellent overlap for $p = 1$ in both cases (fig. 2c/f, for other values for p see SI fig. S9/S13).

For the macrocyclic catalyst **2c**, the linear rate vs. loading behaviour and the catalyst order of $p = 1$ show that this system reacts via the monomeric pathway, independent of catalyst concentration. As for the catenane **1c**, the linear rate vs. loading relationship also indicates that this system consistently follows one catalytic mechanism only, although the catalyst order ($p = 1$) alone does not allow a conclusion if the monomeric or dimeric catalyst pathway is dominating. However, the initial rate of the catenated catalyst **1c** is significantly lower than that of the macrocyclic catalyst **2c** (e.g. $v_0 = 0.88/1.5 \cdot 10^{-7} \text{ M s}^{-1}$ for **1c/2c** at 0.07 mM catalyst loading), despite the fact that the catenated catalyst features two phosphoric acids units. This is in line with the DFT-calculated lower rate for a dimeric catalyst pathway. Based on this combined data, we assume that the dimeric catalysis pathway is dominating for the catenated catalyst **1c** in the first, rate-determining reaction step. In contrast to catalysts **1c/2c**, the acyclic phosphoric acid **3** shows a nonlinear behavior: In the v_0 vs. [3] plot (fig. 3a), increase of catalyst loading leads to a much stronger rate increase at lower loadings than it does at higher loadings.

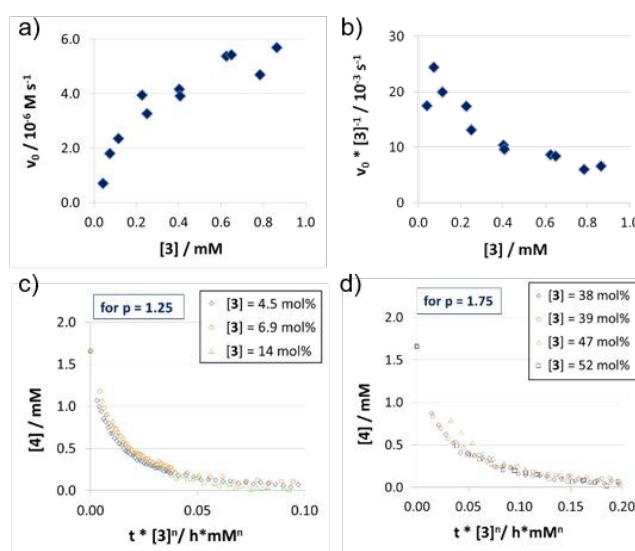


Figure 3: Catalyst order determination for catalyst **3**: Initial rates (a) and normalized initial rates (b) (all at 1.66 mM quinoline **4** and 3.93 mM Hantzsch-ester **7**) and VTNA-plots at low (c) and high (d) catalyst concentrations (selected catalyst concentrations only).

Looking at the normalized initial rates $v_0 / [3]$ (fig. 3b), we found that the normalized rate decreases initially, before it reaches a plateau at higher loadings. In order to see if the nonlinear behavior in rate is due to a change in catalyst order, we performed VTNA. While we find an order of $p = 1.25$ at low catalyst loading, the VTNA clearly shows a larger order of $p = 1.75$ at high catalyst loadings (fig. 3c/d, for other values of p see SI fig. S17/S18). Thus, we believe that the nonlinear behavior of **3** can be interpreted based on competing reaction mechanisms: At low catalyst concentrations, the monomeric



pathway is dominating, although the dimeric pathway still contributes. Vice versa, the dimeric pathway, which involves two phosphoric acids in the rate-determining transition state, dominates at higher catalyst loading.

In order to relate these orders in catalyst to the overall observed reaction rates (as shown in fig. 3a), it must be noted that the rate not only depends on the relative concentrations of the competing rate-determining intermediates (involving one or two catalyst molecules), but also on the corresponding reaction rates of the monomeric and the dimeric pathways.

Normalized reaction rates and influence of dimerization

The normalized initial rates $v_{\text{Norm}} = v_0 / [\text{Cat}]$ (Table 2; also see SI fig. S20) are almost constant for different catalyst loadings in case of **1c/2c** ($v_{\text{Norm}}(\mathbf{1c}) = 1.04 \cdot 10^{-3} \text{ s}^{-1}$, $v_{\text{Norm}}(\mathbf{2c}) = 2.06 \cdot 10^{-3} \text{ s}^{-1}$), as would be expected based on the linear rate vs. loading relationship. In the nonlinear case of catalyst **3**, the maximum initial rate, equivalent to the rate constant for the purely monomeric pathway, can be obtained as the y-intercept in a linear extrapolation for low catalyst loadings ($v_{\text{Max}} = v_{\text{Norm}}(\mathbf{3}_{\text{Mono}}) = 22.7 \cdot 10^{-3} \text{ s}^{-1}$). In turn, the maximum rate for the dimeric pathway can be estimated from the plateau for high catalyst loadings ($v_{\text{Norm}}(\mathbf{3}_{\text{Di}}) = < 6.29 \cdot 10^{-3} \text{ s}^{-1}$).

This shows that there is a smaller difference in normalized initial rates for the macrocycle/catenane pair ($v_{\text{Norm}}(\mathbf{2c})/v_{\text{Norm}}(\mathbf{1c}) = 1.98$) than for the monomeric/dimeric pathway for catalyst **3** ($v_{\text{Norm}}(\mathbf{3}_{\text{Mono}})/v_{\text{Norm}}(\mathbf{3}_{\text{Di}}) = 3.61$). The difference between the macrocyclic and acyclic catalysts is even more pronounced ($v_{\text{Norm}}(\mathbf{3}_{\text{Di}})/v_{\text{Norm}}(\mathbf{1c}) = 6.05$ and $v_{\text{Norm}}(\mathbf{3}_{\text{Mono}})/v_{\text{Norm}}(\mathbf{2c}) = 11.0$), showing that the ethylene-glycol chains significantly reduce the reaction rate (as already seen for the differently sized catenanes **1a/b/c**).

Table 2. Normalized initial rates for **1c/2c/3**.

Catalyst	$v_0 / [\text{Cat}]$ [10^{-3} s^{-1}]
1c	1.04 ^[a]
2c	2.06 ^[a]
3_{Di} (>0.6 mM)	<6.29 ^[b]
3_{Mono} (<0.25 mM)	22.7 ^[c]

[a] Mean value for all catalyst concentrations, [b] Mean value for catalyst concentrations >0.6 mM, [c] Determined as y-intercept in the $v_0 / [\text{Cat}]$ plot for loading <0.25 mM

Detailed analysis for the acyclic phosphoric acid **3**

As detailed above, the nonlinear rate-behavior for the acyclic catalyst **3** can be attributed to both concentration effects and a change in rate constant. At higher concentrations, a smaller number of active species is present (since two molecules of **3** are needed in the dimeric pathway), together with a smaller rate constant for this pathway ($v_{\text{norm}}(\mathbf{3}_{\text{Mono}})/v_{\text{norm}}(\mathbf{3}_{\text{Di}}) = 3.61$, vide supra). Thus, the total rate data (fig. 3) was analyzed in order to determine the mole fractions of catalyst that act via the monomeric and the dimeric pathway, respectively (SI chapter 5). The resulting speciation plot^[26] (fig. 4a) reveals that under the conditions employed (1.66 mM quinoline, 3.93 mM

Hantzsch-ester, toluene solvent), the crossing point of both curves lies at ca. 0.25 mM catalyst (15 mol%). However, taking into account the lower relative rate for the dimeric pathway, the impact of catalyst-dimerization on total rate is less significant (fig. 4b), and only above 0.4 mM, the contribution of the dimeric pathway exceeds that of the monomeric pathway.

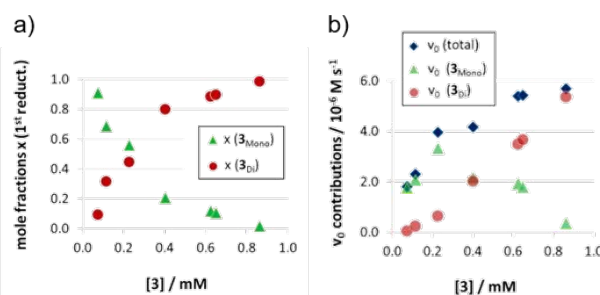


Figure 4: Mole fractions (a) and v_0 contributions (b) for the monomeric and dimeric pathway for different concentrations of catalyst **3** for the first reduction step [$x(\mathbf{3}_{\text{Mono}})$: mole fraction of monomeric catalyst, $x(\mathbf{3}_{\text{Di}})$: mole fraction of phosphoric acid **3** bound in dimeric catalyst].

Second reduction step: Influence of aggregation on stereoselectivity

The rate analysis does not give any insight into the second, stereodetermining reduction step. Thus, we investigated the influence of the overall concentration and of catalyst loading on the enantiomeric excess of the tetrahydroquinoline product **6**, since this gives direct information about the second reduction.

Firstly, we found that at higher overall concentrations (5.0 mM instead of 1.66 mM quinoline), but identical absolute catalyst concentrations, stereoselectivities are shifted towards (*R*)-**6** (e.g. +20%/-22% ee at 25 mM catalyst, meaning 1.5/0.5 mol% loading at 1.66/5.0 mM quinoline concentration, fig.S21b). However, for identical relative catalyst loadings, we find almost identical stereoselectivities (e.g. +72%/+71% ee at 50 mol%, meaning 0.83/2.5 mM catalyst concentration at 1.66/5.0 mM quinoline concentration, fig. S21c). Thus, the stereoselectivity depends mostly on the substrate/catalyst ratio, which would be in line with competing monomeric and dimeric catalyst pathways: High substrate concentrations favour the formation catalyst•dihydroquinoline•Hantzsch-ester complexes at the expense of higher-order catalyst•catalyst•dihydroquinoline•Hantzsch-ester complexes, thus shifting the reaction towards the less stereoselective, monomeric pathway.

Secondly, we checked whether there is a dependence of the stereoselectivity on the conversion, since changing concentrations of substrates **4/7** and products **6/8** might influence the distribution between monomeric and dimeric pathways based on different association constants. However, no change in stereoselectivity was found between 15-95% conversion at 1 mol% catalyst loading (SI table S11 and fig. S25).



Thirdly, we investigated the influence of catalyst loading over a broad concentration range (0.0017 mM to 0.83 mM catalyst concentration, meaning 0.1 to 50 mol% at 1.66 mM quinoline). We observed that there is a drastic change in enantioselectivity (fig. 5): At low catalyst concentrations, the (S)-product enantiomer is favored (-30% ee), while at high catalyst concentrations the selectivity reaches up to 72% ee in favor of the (R)-isomer.

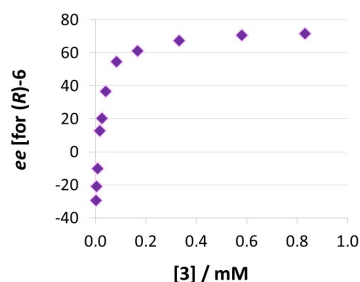


Figure 5: Influence of catalysts loading on enantioselectivities for catalyst **3** (given as enantiomeric excess for (R)-**6**).

This means that the monomeric catalyst and the dimeric pathway not only have different, but actually inverted stereoselectivities. This reflects the enantioselectivities of the macrocyclic and catenated catalysts **2c/1c** (-17% ee/+84% ee), which underpins their predominant reactivity via monomeric (for **2c**) and dimeric (for **1c**) catalytic pathways. A control experiment using 1 mol% phosphoric acid **3** plus 49 mol% benzoic acid (+10% ee, c.f. +13% ee for 1 mol% **3** only) showed that the dimeric pathway requires high concentrations of the phosphoric acid and the same effect cannot easily be achieved when using carboxylic acids as assisting Brønsted-acids (SI table S1).

The strong curvature of the ee vs. [3] curve suggests that the dimeric (more stereoselective) pathway has a stronger contribution in the second reduction step than in the first reduction step. This is in line with our previous DFT-results, which indicate that for the stereodetermining step, the dimeric pathway actually possesses a lower barrier than its monomeric counterpart (6.8 kcal/mol vs. 8.5 kcal/mol).^[17] To generate the corresponding speciation plot, we estimated the relative rates of the monomeric and dimeric pathway based on the DFT-data ($k(\mathbf{3}_{\text{Di}})/k(\mathbf{3}_{\text{Mono}}) = 17.7$, according to $\Delta E_{\text{A}} = 1.7$ kcal/mol)^[17], since this data is not directly available experimentally. The resulting plot shows a different distribution of monomeric and dimeric pathways in comparison to the first reduction step (fig. 6a). The mole fraction of catalyst acting via the dimeric pathway is lower, and the crossing of both curves is observed at ca. 0.5 mM catalyst loading (30 mol%). However, the impact of the dimeric pathway on the second reduction (and thus on the stereoselectivity) is significantly enhanced by its higher relative rate (fig. 6b). Only below a catalyst concentration of 0.012 mM (0.7 mol%), the enantioselectivity is dominated by the monomeric pathway, leading to overall preference for the (S)-product. At 0.17 mM (10 mol%) loading, the

stereoselectivity already reaches 61% ee for the (R) isomer, which is close to the highest stereoselectivity of 72% observed at 0.83 mM (50 mol%) loading. This demonstrates the relative importance of the dimeric pathway in terms of stereoselectivity, even at low catalyst loadings.

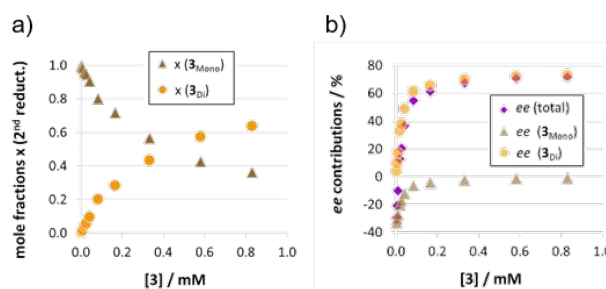


Figure 6: Mole fractions and ee contributions for the monomeric and dimeric pathway for different concentrations of catalyst **3** for the second reduction step.

NMR-spectroscopic investigation of catalyst dimerization

Model systems and experimental conditions

Next, detailed NMR-spectroscopic studies were performed to elucidate the structural space including the dimeric reaction pathway for acyclic catalyst **3**. Temperatures between 180-200 K were used to sufficiently slow down exchange processes and to detect separated hydrogen bonded protons (SI fig. S26). Since in toluene **3** was nearly insoluble at these temperatures, CD_2Cl_2 was used, which provided sufficient solubility and signal dispersion (for spectra and solvents see SI fig. S27).^[27] In addition, DFT-calculations at the TPSS-D3/def2-QZVP+COSMO-RS//TPSS-D3/def2-SVP+DCOSMO-RS level of theory^[28] showed that analogous species should be present in CD_2Cl_2 and toluene (SI chapter 7). Experimentally, we verified that in dichloromethane there is also a strong influence of catalyst loading on enantioselectivities. As expected by DFT, the absolute stereoselectivities in dichloromethane are lower (-33% to -6% ee for 1-50 mol% catalyst loading, SI fig. S28), nevertheless showing that competing monomeric and dimeric pathways are also operating in dichloromethane.

For the structural NMR-investigations, quinolines **4b-d** (fig. 7a) were selected as model substrates, as they possess suitable probes for ^1H and ^{19}F NMR spectroscopy. Furthermore, they modulate the basicity of the quinoline and thus allow for an alteration of the hydrogen bond strength. Samples with a 1:1 or 2:1 stoichiometry of **3:4b-d** at NMR suitable concentrations (10-50 mM of **3**) were employed to study the structures of the complex **3•Qu** or the complex **3•3•Qu**, respectively.

1:1 stoichiometries (3•Qu complexes)

To shed light on the structures involved in the monomeric catalysis pathway, samples of **3** and **4b-d** with a 1:1 stoichiometry were investigated. For **4b**, only one hydrogen bond proton signal was detected at 16.83 ppm (fig. 7b), which is a typical chemical shift for protons in strong hydrogen bonds



and similar to the hydrogen bond signals in CPA•imine complexes.^{[13],[29]} The detection of magnetization transfers between the H-bond proton and both quinoline and CPA further corroborated the assignment of this hydrogen bond signal (SI fig. S30). The presence of the **3•4b** complex was further validated by diffusion ordered spectroscopy (DOSY) measurements. Similar hydrodynamic radii for **3** (9.11±0.17 Å) and **4b** (7.2±1.62 Å) revealed the dominant presence of the complex and are in the same order as the radii of CPA•imine complexes.^[15] Using different homo- and heteronuclear 2D spectra, a chemical shift assignment of **3•4b** could be accomplished (SI fig. S29) as well as an in-depth NOE analysis (SI fig. S32). Two different conformations with a ≈180° rotated orientation of the quinolines were identified, which are on a fast exchange on the NMR time scale^{[14],[15],[30]} (SI fig. S32 for a more detailed description of the structures and exchange pathway).^[15] One of the conformations validated the previously computed structure of the **3•Qu** complex.^[17]

Similar ¹H spectra were obtained with quinolines **4c** and **4d**. Decreasing the basicity of the quinoline resulted in low field shifted proton signals (**4b**: 16.83 ppm, **4c**: 17.42 ppm, **4d**: 18.08 ppm; SI fig. S31), which corresponds to an increase in hydrogen bond strength.^[31] Thus, similar to CPA•imine complexes,^{[13],[29b]} CPA•Qu complexes are present as hydrogen bond assisted ion pairs anchored by a strong, charge assisted hydrogen bond.^{[13],[29b]} At 1:1 ratios, higher aggregates, such as **3•3•Qu** complexes are below the NMR-detection limit. In summary, monomeric **3•Qu** complexes are analogous to the previously investigated CPA•imine systems^{[13],[14],[15],[29b],[30]} and are at least for the monomeric pathway a representative for catalyst•substrate complexes in CPA catalyzed transformations.

2:1 stoichiometries (**3•3•Qu** complexes)

In order to populate and characterize the **3•3•Qu** complex (fig. 7a), samples with a 2:1 stoichiometry of **3** to **4b-d** were investigated. For quinoline **4b**, three dominant hydrogen bonded protons with a ratio of H¹ : H² : H³ ≈ 1 : 2.4 : 2.4 were observed (fig. 7b).^[32] Proton H¹ corresponds to the **3•4b** complex, as it has a nearly identical chemical shift as the H-bond proton in the respective sample with a 1:1 stoichiometry (Δδ(¹H) = 0.07 ppm). Protons H² and H³ have similar integrals, which fits the expected hydrogen bonding situation for the **3•3•4b** complex. Proton H¹ and H³ showed exchange signals in the NOE spectrum (SI fig. S33). In addition, both protons show similar low field shifts with quinolines **4c** and **4d**, i.e. a similar modulation of the H-bond strength (SI fig. S31).

Thus, proton H³ is assigned to the PO...H-N⁺ hydrogen bond (fig. 7b, highlighted in blue) and proton H² to the PO...H-OP hydrogen bond (fig. 7b, highlighted in red) of the **3•3•4b** complex. The significant high field shift of proton H³ compared to proton H¹ reveals a weaker PO...H-N⁺ hydrogen bond, i.e. a stronger proton transfer on the quinoline in the **3•3•4b** complex compared to the **3•4b** complex.^[31] This weakening is often found in bifurcated hydrogen bonds^[29a] and can be rationalized by the compensation of an increasing

negative partial charge on the phosphate by the additional PO...H-OP hydrogen bond enabled by the second CPA.

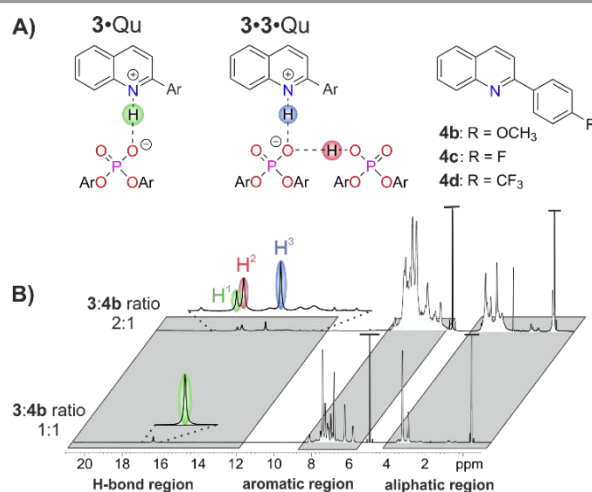


Figure 7: a) Schematic structures of the **3•Qu** and **3•3•Qu** complexes and substituents of quinolines **4b-d**. b) Spectral resolution of the ¹H spectra of complexes of **3** and **4b** at a 1:1 or 2:1 stoichiometry at 200 K and 600 MHz in CD₂Cl₂. In the 1:1 system, only one H-bond is detected, presumably of the **3•4b** complex. For the 2:1 system, three major H-bonds are observed at 16.76 (H¹), 16.51 (H²) and 15.27 ppm (H³), most likely of the **3•4b** (H¹) and **3•3•4b** (H², H³) complex.

For CPA•imine systems, a correlation between hydrogen bond strength and reactivity has been observed previously, giving lower reactivities for weaker hydrogen bonds.^[13] This trend is also reflected for the monomeric and dimeric reaction pathway in the investigated quinoline systems, as the dimeric reaction pathway featuring a weaker PO...H-N⁺ hydrogen bond shows lower reaction rates than the monomeric pathway (fig. 8).

Moreover, additional hydrogen bond signals were observed in the ¹H spectrum at a 2:1 stoichiometry, which are low populated and/or have severe line broadening (fig. 7b, magnified H-bond region). EXSY signals in the NOESY spectrum revealed, that these signals are in chemical exchange with the PO...H-N⁺ or PO...H-OP hydrogen bond protons of the **3•4b** and **3•3•4b** structures, thus suggesting the presence of different/higher aggregates of **3** and **4b**. Additional detailed NMR-structural analysis of the **3•3•4b** complex could not be achieved due to strong line broadening and signal overlaps (see aromatic region in fig. 7b).

Similar ¹H spectra were obtained for quinolines **4c** and **4d** (SI fig. S31). Measurements at lower temperatures were not fruitful due to the poor solubility of **3** in the required freonic mixtures^[27] (CDCl₂F, CDClF₂). However, the spectra at 300 K were significantly simplified and better resolved, as the different species (free **3** and Qu, **3•Qu**, **3•3•Qu** and potential higher aggregates) are in fast exchange on the NMR time scale. DOSY measurements were performed at a 1:1 and 2:1 stoichiometry to further confirm the postulated presence of **3•3•4b** in the 2:1 samples (SI table S13). Due to the chemical exchange of the different species, the measured diffusion coefficients and derived hydrodynamic radii are an average of the values of the different species, weighted by their respective population and lifetime.^[33] Similar hydrodynamic



radii were derived for the quinoline and the CPA, demonstrating that also at 300 K the catalyst-quinoline complexes are the dominant species (SI table S14). When comparing the derived hydrodynamic radii for the 1:1 and 2:1 stoichiometries, a size increase of ≈ 2.2 and 3.2 \AA was observed for the quinolines **4b** and **4c** in the 2:1 samples, which is in agreement with the previously reported offset for CPA•Imine complexes and their dimers ($\approx 3 \text{ \AA}$).^[15] The increased radii clearly show, that higher aggregates, such as the **3•3•Qu** complex are populated when employing a 2:1 ratio of catalyst and quinoline.

Overall mechanistic picture for catalyst **3**

In summary, our combined kinetic, stereoselectivity, DFT and NMR analysis of the transfer-hydrogenation of quinolines with the acyclic catalyst **3** has revealed the following key findings (also see fig. 8):

- The catalytic reaction using catalyst **3** involves competing monomeric and dimeric pathways, as found by analysis of the kinetics and stereoselectivity and by DFT.

- Both the **3•Qu** and **3•3•Qu** complexes, which are relevant for the monomeric and dimeric pathway, were directly observed by low-temperature NMR-spectroscopy.

- For the first reduction step (**4** to **5**), kinetics, H-bond analysis and DFT jointly show that the reduction occurs faster for the monomeric catalyst than for the dimeric one (cycles M1 and D1, fig. 8). For this reason, the influence of the dimeric pathway on the reaction rate is less pronounced and the dimeric pathway only dominates above 0.25 mM / 15 mol% catalyst.

- For the second, stereoselective reduction step, the effect of catalyst concentration on stereoselectivity shows that the monomeric and dimeric pathways not only have different, but even inversed stereoselectivities. This reflects the selectivities of the macrocyclic and catenated catalysts **1c/2c**.

- As corroborated by DFT, the stereoselective second reduction (**5** to **6**) occurs faster for the dimeric pathway (cycles M2 and D2, fig. 8). Thus, the impact of catalyst dimerization on the stereo-selectivity is much more pronounced, with the dimeric pathway dominating even at catalyst loading as low as 0.012 mM (0.7 mol%).

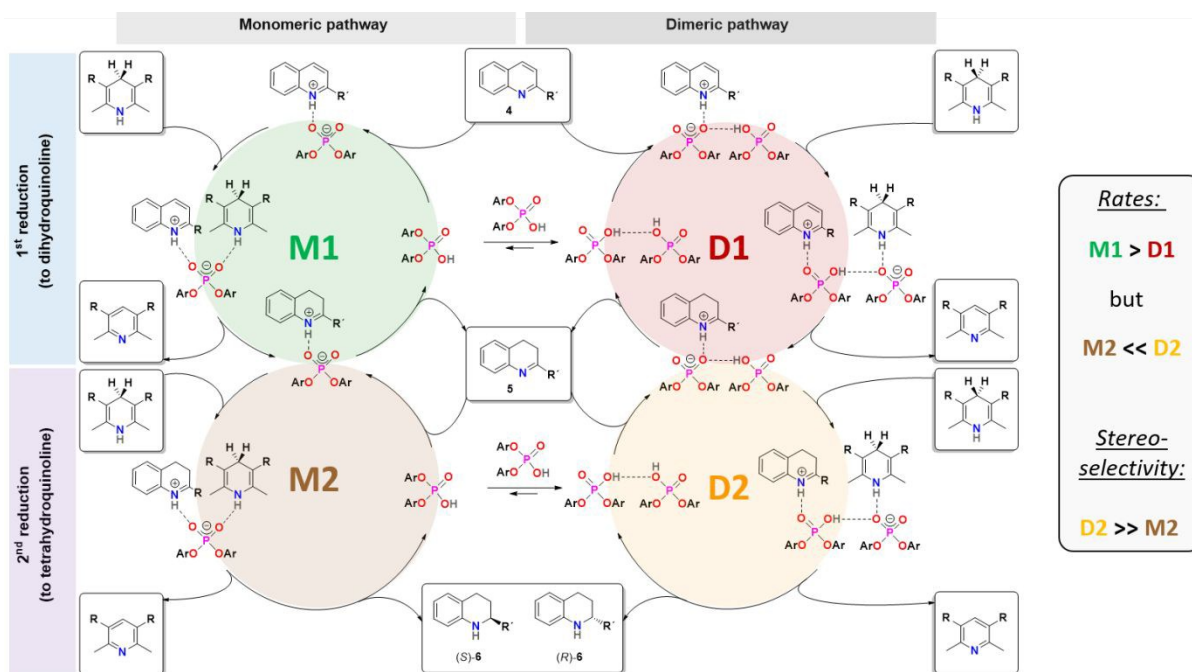


Figure 8: Revised mechanistic picture for the transfer-hydrogenation of quinolines catalyzed by chiral phosphoric acids.

Conclusion

In conclusion, we have elucidated the importance of acid-acid interactions in phosphoric-acid based organocatalysis, using the transfer-hydrogenation of quinolines as an example. Based on a detailed mechanistic analysis of the catenated, macrocyclic and acyclic phosphoric acids **1/2/3**, we established that the catalytic reactions in case of the catenated and macrocyclic catalysts **1/2** are dominated by the dimeric and the monomeric pathway, respectively. In stark contrast, but consistent with our recent DFT-work, the acyclic phosphoric

acid **3** shows a concentration-dependent change in the reaction mechanism, involving either one or two catalyst molecules in the rate- or and stereodetermining intermediates. The formation of complexes involving two catalyst species and one quinoline molecule was directly proven by NMR-spectroscopy. While the influence of these intermolecular acid-acid interactions on reaction kinetics is moderate, the impact on stereoselectivity is very pronounced, even leading to opposite enantioselectivities for the monomeric (-30% ee) and the dimeric catalysis pathway (+72% ee). Based on these findings, we elaborated a revised



mechanism for the phosphoric acid catalyzed transfer hydrogenation of quinolines.

In comparison to other phosphoric-acid catalyzed transfer hydrogenations, it becomes clear that acid-acid interactions may well be relevant in these cases as well.^{[4],[34]} While we find a significant effect on the dimeric pathway at concentrations as low as 0.012 mM, commonly employed catalyst concentrations in the literature are significantly higher (ranging from 1 mM^{[4],[34a],[34g]} to 2 mM^[34d-f] 8 mM^[34c] or even 10 mM^[34b]). Certainly, the extent of intermolecular acid-acid interactions will depend strongly on the catalyst structure and has been shown to be lower for bulky phosphoric acids such as TRIP.^[35] In addition, other factors such as the substrate structures and the solvent may favour or disfavour the formation of higher aggregates. Nevertheless, dimeric catalysis pathways may be relevant, if not dominating, in other phosphoric-acid catalyzed transformations as well. We are currently investigating the influence of acid-acid interactions for other catalyst structures and other catalytic reactions in our laboratory, since the better understanding of such supramolecular interactions may have a major impact for the future development of phosphoric-acid catalyzed asymmetric transformations.

Conflicts of interest

There are no conflicts to declare.

Acknowledgements

Funding by the Fonds der Chemischen Industrie (Liebig-Fellowship to J.N.) and the German Research Foundation (DFG, NI1273/2-1) is gratefully acknowledged. J. N. would like to thank Prof. Carsten Schmuck for his support.

J. G. thanks the Fonds der Chemischen Industrie for funding (Kekulé-Fellowship). J.G., H. Z., R. M. G. and S. G. thank the German Research Foundation (SPP 1807/2 Dispersion) for funding.

§ In memory of Prof. Carsten Schmuck.

Notes and references

- 1 A. Berkessel and H. Gröger, *Asymmetric Organocatalysis - From Biomimetic Concepts to Applications in Asymmetric Synthesis*, Wiley-VCH, Weinheim, 2005.
- 2 List's proline-catalyzed aldol reactions (see ref. [3]) uses 30-40 mM catalyst, while Rueping's phosphoric acid catalyzed hydrogenation of quinolines (see ref. [4a]) uses 1-5 mM catalyst.
- 3 B. List, R. A. Lerner and C. F. Barbas, *J. Am. Chem. Soc.*, 2000, **122**, 2395-2396.
- 4 a) M. Rueping, A. P. Antonchick, T. Theissmann, *Angew. Chem. Int. Ed.*, 2006, **45**, 3683-3686; b) M. Rueping, A. P. Antonchick and T. Theissmann, *Angew. Chem. Int. Ed.*, 2006, **45**, 6751-6755.
- 5 D. D. Ford, D. Lehnerr, C. R. Kennedy and E. N. Jacobsen, *J. Am. Chem. Soc.*, 2016, **138**, 7860-7863.
- 6 C. R. Kennedy, D. Lehnerr, N. S. Rajapaksa, D. D. Ford, Y. Park and E. N. Jacobsen, *J. Am. Chem. Soc.*, 2016, **138**, 13525-13528.
- 7 Y. Park, K. C. Harper, N. Kuhl, E. E. Kwan, R. Y. Liu and E. N. Jacobsen, *Science*, 2017, **355**, 162-166.
- 8 a) S. H. Oh, H. S. Rho, J. W. Lee, J. E. Lee, S. H. Youk, J. Chin and C. E. Song, *Angew. Chem. Int. Ed.*, 2008, **47**, 7872-7875; b) H. S. Rho, S. H. Oh, J. W. Lee, J. Y. Lee, J. Chin and C. E. Song, *Chem. Commun.*, 2008, 1208-1210; c) H. B. Jang, H. S. Rho, J. S. Oh, E. H. Nam, S. E. Park, H. Y. Bae and C. E. Song, *Org. Biomol. Chem.*, 2010, **8**, 3918-3922; d) G. Tárkányi, P. Király, T. Soós and S. Varga, *Chem. Eur. J.*, 2012, **18**, 1918-1922; e) R. Salvio, L. Massaro, A. Puglisi, L. Angelini, A. Antenucci, S. Placidi, F. Sciubba, L. Galantini and M. Bella, *Org. Biomol. Chem.*, 2018, **16**, 7041-7049.
- 9 a) D. Parmar, E. Sugiono, S. Raja and M. Rueping, *Chem. Rev.*, 2014, **114**, 9047-9153; b) D. Parmar, E. Sugiono, S. Raja and M. Rueping, *Chem. Rev.*, 2017, **117**, 10608-10620; c) L. Schreyer, R. Properzi and B. List, *Angew. Chem. Int. Ed.*, 2019, **58**, 12761-12777.
- 10 N. Li, X.-H. Chen, S.-M. Zhou, S.-W. Luo, J. Song, L. Ren and L.-Z. Gong, *Angew. Chem. Int. Ed.*, 2010, **49**, 6378-6381.
- 11 C. Detering, P.M. Tolstoy, N.S. Golubev, G.S. Denisov and H.-H. Limbach, *Dokl. Phys. Chem.*, 2001, 353-356.
- 12 C. Malm, H. Kim, M. Wagner and J. Hunger, *Chem. Eur. J.*, 2017, **23**, 10853-10860.
- 13 K. Rothermel, M. Melikian, J. Hioe, J. Greindl, J. Gramüller, M. Žabka, N. Sorgenfrei, T. Hausler, F. Morana and R. M. Gschwind, *Chem. Sci.*, 2019, **114**, 1929.
- 14 J. Greindl, J. Hioe, N. Sorgenfrei, F. Morana and R. M. Gschwind, *J. Am. Chem. Soc.*, 2016, **138**, 15965-15971.
- 15 M. Melikian, J. Gramüller, J. Hioe, J. Greindl, R. M. Gschwind, *Chem. Sci.*, 2019, **10**, 5226-5234.
- 16 R. Mitra, M. Thiele, F. Octa-Smolín, M. C. Letzel and J. Niemeyer, *Chem. Commun.*, 2016, **52**, 5977-5980.
- 17 R. Mitra, H. Zhu, S. Grimme and J. Niemeyer, *Angew. Chem. Int. Ed.*, 2017, **56**, 11456-11459.
- 18 For reviews on acid-acid interactions in organocatalysis see: a) H. Yamamoto and K. Futatsugi, *Angew. Chem. Int. Ed.*, 2005, **44**, 1924-1942; b) C. Min and D. Seidel, *Chem. Soc. Rev.*, 2017, **46**, 5889-5902; c) R. Mitra and J. Niemeyer, *ChemCatChem*, 2018, **10**, 1221-1234.
- 19 C. L. Perrin, *J. Chem. Educ.*, 2017, **94**, 669-672.
- 20 a) D. G. Blackmond, *Angew. Chem. Int. Ed.*, 2005, **44**, 4302-4320; b) J. S. Mathew, M. Klussmann, H. Iwamura, F. Valera, A. Futran, E. A. C. Emanuelsson and D. G. Blackmond, *J. Org. Chem.*, 2006, **71**, 4711-4722.
- 21 a) J. Burés, *Angew. Chem. Int. Ed.*, 2016, **55**, 16084-16087; b) J. Burés, *Angew. Chem. Int. Ed.*, 2016, **55**, 2028-2031; c) C. D.-T. Nielsen and J. Burés, *Chem. Sci.*, 2019, **10**, 348-353.
- 22 The translation of the concentration vs. time profiles into reaction rates adds additional inaccuracy in the data analysis. This is avoided by directly using concentration vs. time profiles in VTNA instead of using rate vs. time profiles in classical RPKA.
- 23 Yields for **1b/2b** are lower than reported earlier (14%/22%) [see ref. 11]. We attribute this to a different chromatography system that was used for this work.
- 24 a) J. P. Reid and J. M. Goodman, *Org. Biomol. Chem.*, 2017, **15**, 6943-6947; b) J. P. Reid and J. M. Goodman, *Chem. Eur. J.*, 2017, **23**, 14248-14260; c) J. P. Reid, L. Simón and J. M. Goodman, *Acc. Chem. Res.*, 2016, **49**, 1029-1041; d) L. Simón and J. M. Goodman, *J. Am. Chem. Soc.*, 2008, **130**, 8741-8747; e) Y. Shibata and M. Yamanaka, *J. Org. Chem.*, 2013, **78**, 3731-3736; f) T. Marcelli, P. Hammar and F. Himo, *Chem. Eur. J.*, 2008, **14**, 8562-8571.
- 25 J. Pastor, E. Rezabal, A. Voituriez, J.-F. Betzer, A. Marinetti and G. Frison, *J. Org. Chem.*, 2018, **83**, 2779-2787.



- 26 For the dimeric catalyst, the mole fraction represents the amount of catalyst that is bound in the dimeric catalyst (meaning that the molar amount of dimeric catalyst is half of the molar amount of phosphoric acid as expressed by the mole fraction)
- 27 J. S. Siegel and F. A. L. Anet, *J. Org. Chem.*, 1988, **53**, 2629-2630.
- 28 a) S. Grimme, C. Bannwarth and P. Shushkov, *J. Chem. Theory. Comput.*, 2017, **13**, 1989-2009; b) S. Grimme and C. Bannwarth, *J. Chem. Phys.*, 2016, **145**, 054103; c) P. Shushkov and S. Grimme, unpublished; d) TURBOMOLE V7.0 2015, a development of University of Karlsruhe and Forschungszentrum Karlsruhe GmbH, 1989-2007, TURBOMOLE GmbH, since 2007; available from <http://www.turbomole.com>; e) J. M. Tao, J. P. Perdew, V. N. Staroverov and G. E. Scuseria, *Phys. Rev. Lett.*, 2003, **91**, 146401; f) S. Grimme, J. Antony, S. Ehrlich and H. Krieg, *J. Chem. Phys.* 2010, **132**, 154104; g) S. Grimme and L. Goerigk, *J. Comput. Chem.*, 2011, **32**, 1456-1465; h) A. Schäfer, H. Horn and R. Ahlrichs, *J. Chem. Phys.*, 1992, **97**, 2571; i) F. Weigend, *Phys. Chem. Chem. Phys.*, 2006, **8**, 1057; j) S. Sinnecker, A. Rajendran, A. Klamt, M. Diedenhofen and F. Neese, *J. Phys. Chem. A*, 2006, **110**, 2235-2245; h) A. Klamt and G. Schüürmann, *J. Chem. Soc., Perkin Trans.*, 1993, **2**, 799-805; i) K. Eichkorn, F. Weigend, O. Treutler and R. Ahlrichs, *Theor. Chem. Acc.*, 1997, **97**, 119-124; j) P. Deglmann, K. May, F. Furche and R. Ahlrichs, *Chem. Phys. Lett.*, 2004, **384**, 103-107; k) S. Grimme, *Chem. Eur. J.*, 2012, **18**, 9955-9964; l) F. Weigend, F. Furche and R. Ahlrichs, *J. Chem. Phys.*, 2003, **119**, 12753; m) F. Eckert and A. Klamt, COSMOtherm, Version C3.0, Release 14.01; COSMOlogic GmbH & Co. KG, Leverkusen, Germany, 2013; n) A. Klamt, *J. Phys. Chem.*, 1995, **99**, 2224-2235; o) F. Eckert and A. Klamt, *AIChE Journal*, 2002, **48**, 369-385.
- 29 a) T. Steiner, *Angew. Chem. Int. Ed.*, 2002, **41**, 48-76; b) N. Sorgenfrei, J. Hioe, J. Greindl, K. Rothermel, F. Morana, N. Lokesh and R. M. Gschwind, *J. Am. Chem. Soc.*, 2016, **138**, 16345-16354.
- 30 N. Lokesh, J. Hioe, J. Gramüller and R. M. Gschwind, *J. Am. Chem. Soc.*, 2019, **141**, 16398-16407.
- 31 S. Sharif, G. S. Denisov, M. D. Toney and H.-H. Limbach, *J. Am. Chem. Soc.*, 2007, **129**, 6313-6327.
- 32 The experimentally observed thermodynamic preference for the complex **3•4b** ($\Delta G_{\text{exp}}(\mathbf{3}\cdot\mathbf{3}\cdot\mathbf{4b} - \mathbf{3}\cdot\mathbf{4b}) = -1.5$ kJ) is qualitatively represented in the theoretical calculations, although by far less pronounced ($\Delta G_{\text{theor}}(\mathbf{3}\cdot\mathbf{3}\cdot\mathbf{4b} - \mathbf{3}\cdot\mathbf{4b}) = -12.2$ kJ). Such a significant quantitative offset between experiment and computations was also found for CPA•imine systems and probably originates in dispersion interactions with the solvent (see reference 15).
- 33 a) E. J. Cabrita and S. Berger, *Magn. Reson. Chem.*, 2002, **40**, 122-127; b) C. T.W. Moonen, P. van Gelderen, G. W. Vuister and P. C.M. van Zijl, *J. Magn. Res.*, 1992, **97**, 419-425.
- 34 a) S. Hoffmann, A. M. Seayad and B. List, *Angew. Chem. Int. Ed.*, 2005, **44**, 7424-7427; b) M. Rueping, E. Sugiono, C. Azap, T. Theissmann and M. Bolte, *Org. Lett.*, 2005, **7**, 3781-3783; c) R. I. Storer, D. E. Carrera, Y. Ni and D. W. C. MacMillan, *J. Am. Chem. Soc.*, 2006, **128**, 84-86; d) G. Li and J. C. Antilla, *Org. Lett.*, 2009, **11**, 1075-1078; e) A. Aillerie, V. L. de Talancé, A. Moncomble, T. Bousquet and L. Pélineski, *Org. Lett.*, 2014, **16**, 2982-2985; f) X.-F. Cai, R.-N. Guo, G.-S. Feng, B. Wu and Y.-G. Zhou, *Org. Lett.*, 2014, **16**, 2680-2683; g) Y. Zhang, R. Zhao, R. L.-Y. Bao and L. Shi, *Eur. J. Org. Chem.*, 2015, 3344-3351.
- 35 a) M. R. Monaco, D. Fazzi, N. Tsuji, M. Leutzsch, S. Liao, W. Thiel and B. List, *J. Am. Chem. Soc.*, 2016, **138**, 14740-14749; b) For a review including the crystal structure of the TRIP-

dimer see: M. R. Monaco, G. Pupo and B. List, *Synlett*, 2016, **27**, 1027-1040.

DOI: 10.1039/D0SC01026J



ARTICLE

Entry for the Table of contents:

Supramolecular acid-acid interactions lead to competing monomeric and dimeric pathways in phosphoric acid catalysis – so that stereoselectivities depend on catalyst concentration

